2014

Condensation and Evaporation of R134a, R1234ze(E) and R1234ze(Z) Flow in Horizontal Microfin Tubes at Higher Temperature

Chieko Kondou
Kyushu University, Japan, kondo.chieko.162@m.kyushu-u.ac.jp

Fumiya Mishima
Kyushu University, Japan, mishima@phase.cm.kyushu-u.ac.jp

JinFan Liu
Kyushu University, Japan, liu@phase.cm.kyushu-u.ac.jp

Shigeru Koyama
Kyushu University, Japan, koyama@cm.kyushu-u.ac.jp

Condensation and Evaporation of R134a, R1234ze(E) and R1234ze(Z) Flow in Horizontal Microfin Tubes at Higher Temperatures

Chieko KONDOU[1]*, Fumiya MISHIMA[1], JinFan LIU[1], Shigeru KOYAMA[1, 2]

[1] Kyushu University, Interdisciplinary Graduate School of Engineering Science, Fukuoka, Japan
*kondo.chieko.162@m.kyushu-u.ac.jp

[2] Kyushu University, International Institute for Carbon-Neutral Energy Research, Fukuoka, Japan
koyama@phase.cm.kyushu-u.ac.jp

*Corresponding Author

ABSTRACT

The hydrofluoro-olefins R1234ze(E) and R1234ze(Z) are anticipated to be environmentally friendly working fluids for industrial high-temperature heat pumps. This study presents the experimental data obtained for the heat transfer coefficient and pressure gradient of these refrigerants in a horizontal microfin tube measured at temperatures of 65 °C for condensation and 30 °C for evaporation. For condensation, the heat transfer coefficient and pressure gradient of R1234ze(Z) are higher than those of R1234ze(E), mainly because of the higher vapor velocity due to the lower vapor density, higher liquid thermal conductivity and latent heat compared with those of R134a and R1234ze(E). For evaporation, the heat transfer coefficient of R1234ze(Z) was somewhat higher than those of R134a and R1234ze(E), but only for higher vapor qualities. However, the pressure gradient of R1234ze(Z) was notably higher than that of R134a and R1234ze(E). A comparison between experimental and predicted values validated that the heat transfer coefficient (HTC) and pressure gradient of R1234ze(E) and R123ze(E) can be accurately predicted using existing correlations and currently available predictions for thermophysical properties.

1. INTRODUCTION

From an environmental perspective, switching from conventional refrigerants to low-GWP (global warming potential) refrigerants is the most important consideration for heat pump systems. Therefore, new low-GWP refrigerants made from fluorinated olefins, such as R1234ze(E) and the isomer R1234ze(Z), have been investigated in recent years. Brown *et al*. (2009, 2010) comparatively surveyed the thermophysical properties of new refrigerants, including R1234ze(E) (GWP=6), which has very similar properties and could serve as an alternative to R134a (GWP = 1300), and R1234ze(Z) (expected the GWP less than 10), which is most likely suitable for high-temperature heat pumps. According to the brief risk assessment conducted by Koyama *et al*. (2013), the flammability of R1234ze(Z) seems to be very mild, and the acute inhalation toxicity is very likely negative. Akasaka *et al*. (2013) proposed an equation of state for R1234ze(Z) to fit the measured thermodynamic properties provided by Higashi *et al*. (2013). Based on this equation, the fluid file was provided so that the properties can be calculated on REFPROP (Lemmon *et al*., 2013). The transport properties calculated according to the corresponding states principle of the provided fluid file agree with the thermal conductivity and viscosity measured by Miyara *et al*. (2013). Fukuda *et al*. (2014) numerically quantified the irreversible loss and suggested that R1234ze(Z) is likely beneficial to high-temperature heat pumps. However, the heat transfer data of these new refrigerants for such high-temperature conditions is not yet available in the open literature. Based on above significance, this paper presents the pressure gradient and heat transfer data during the condensation and evaporation in a horizontal microfin tube for R1234ze(Z), R1234ze(Z) and R134a.

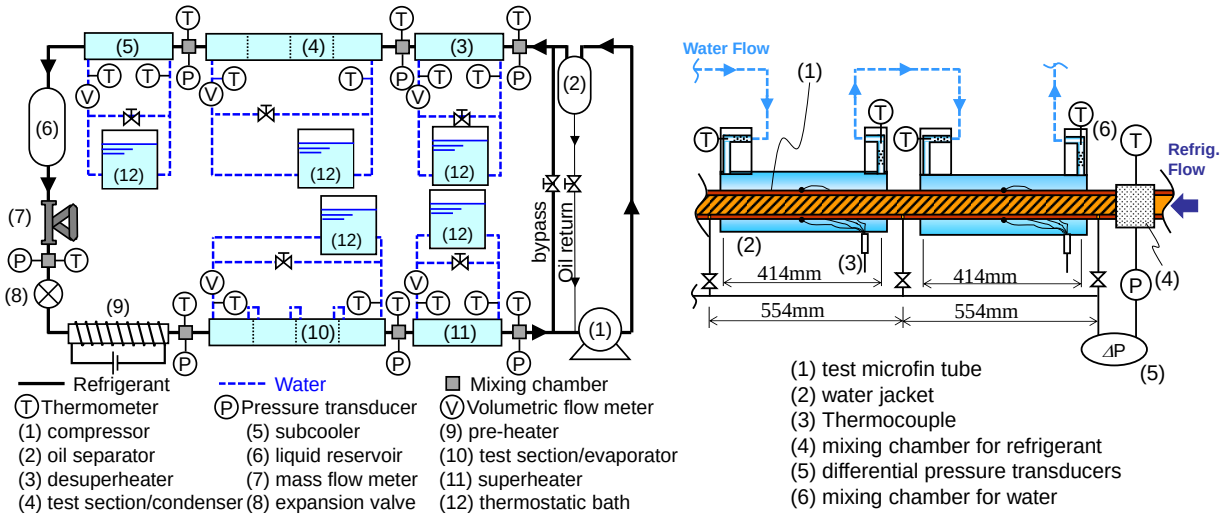

(a) diagram of the test loop (b) structure of the test section (for condensation test)

Figure 1: Experimental apparatus

2. EXPERIMENTAL METHOD

Figure 1 (a) illustrates a vapor compression cycle used for the experiment. Heat transfer coefficient (HTC) and pressure gradient are measured in test sections (4) and (10) for condensation and evaporation, respectively. To determine the bulk enthalpies of superheated vapor, the bulk mean temperature and the pressure are measured in mixing chambers placed at the inlet of the desuperheater (3) and the outlet of the superheater (11). Based on these enthalpies, the enthalpies in the test sections are calculated by considering the enthalpy changes in the desuperheater and superheater obtained from the water side of the heat balance. As schematically outlined in Figure 1 (b), a horizontally placed test microfin tube is surrounded by four water jackets and bored 0.6 mm ID pressure ports in the test section to measure the heat transfer rates over the 414-mm length and pressure drops at 554 mm intervals. At the center of each subsection (i.e., the water jacket), four thermocouples are attached to the tube outer surface. The internal tube surface temperature, T_{wi}, is obtained from the one-dimensional heat conduction in the tube wall.

$$T_{wi} = \left(T_{wo,top} + T_{wo,bottom} + T_{wo,right} + T_{wo,left}\right)/4 - \left[Q_{H2O\,TS}/\left(2\pi \Delta Z \lambda_{tube}\right)\right]\ln\left(D_o/d_{eq}\right) \quad (1)$$

The representative refrigerant temperature of each subsection, $T_{r\,TS}$, is defined as the arithmetic mean of the inlet and outlet calculated from the enthalpies and pressures by assuming thermodynamic equilibrium.

$$T_{r\,TS} = \left(T_{r\,TS,i} + T_{r\,TS,o}\right)/2 \quad (2)$$

$$T_{r\,TS,i} = f_{equilibrium}\left(h_{r\,TS,i}, P_{r\,TS,i}\right) \quad (3)$$

$$T_{r\,TS,o} = f_{equilibrium}\left(h_{r\,TS,o}, P_{r\,TS,o}\right) \quad (4)$$

Table 1 specifies the dimensions of the test microfin tube referring the symbols in the microscopic cross sectional area of Figure 2. The equivalent inner diameter, d_{eq}, is the diameter of a smooth tube that envelops an equal free flow volume. The surface enlargement, η_A, is the ratio of the actual heat transfer area to that of the equivalent smooth tube. Based on the actual heat transfer area, the heat flux, q, and the HTC, α, are defined as follows:

$$q_{TS1} = Q_{H2O\,TS1}/\left(\pi d_{eq} \eta_A \Delta Z\right) \quad (5)$$

$$\alpha_{TS1} = q_{TS1}/\left(T_{r\,TS1} - T_{wi}\right) \quad (6)$$

A deviation within 1 kW m^{-2} of the targeted average heat flux was allowed to adjust for the test conditions, except for the dry-out condition during the evaporation. The condensation and evaporation tests were carried out at saturation temperatures of 65 and 30 °C. The conditions are considered for industrial high-temperature heat pumps, which are

Table 1: Dimensions of test microfin tube

Outer diameter	D_o	6.0	mm
Fin root inner diameter	d_{max}	5.45	mm
Equivalent inner diameter	d_{eq}	5.35	mm
Fin height	h_{fin}	0.255	mm
Helix angle	β	20	deg.
Number of fins	N_{fin}	48	-
Surface enlargement	η_A	2.24	-

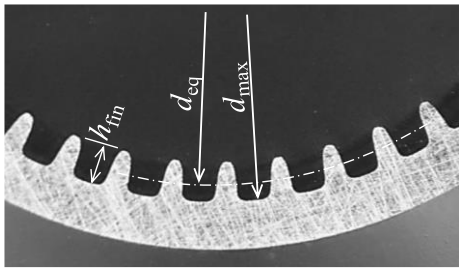

Figure 2: Microscopic cross section of the tube.

Table 2: Comparison on thermophysical properties between R134a, R1234ze(E) and R1234ze(Z)

Refrigerant name		R134a	R1234ze(E)	R1234ze(Z)
ODP / GWP_{100}		0 / 1430*[b]	0 / 6*[c]	0 / <10*[d]
Safety group (ANSI/ASHRAE 34-2007)		A1	A2L	A2L(expected)*[d]
Normal boiling temperature		-26.4	-19.3	9.4
Critical temperature		101.1	109.4	150.1
at 65 °C	Pressure [MPa]	1.89	1.44	0.59*[e]
	Density [kg m^{-3}] *[a]	100/1026	80.1/1010	28.6/1107*[e]
	Viscosity [μPa s] *[a]	14.0/115	14.4/122	12.6/191*[e]
	Thermal conductivity [mW m^{-1} K^{-1}] *[a]	19.3/63.9	18.0/61.3	16.0/76.4*[e]
	Latent heat of vaporization [kJ kg^{-1}]	132.1	129.9	177.8*[e]
at 30 °C	Pressure [MPa]	0.77	0.58	0.210*[e]
	Density [kg m^{-3}] *[a]	38/1187	30.5/1146	10.4/120*[e]
	Viscosity [μPa s] *[a]	11.9/183	12.5/188	11.3/277*[e]
	Thermal conductivity [mW m^{-1} K^{-1}] *[a]	14.3/79	14/72.5	12.9/87.6*[e]
	Latent heat of vaporization [kJ kg^{-1}]	173.1	163.1	202.9*[e]

*[a] These data at the equilibrium state are listed in the manner of "vapor / liquid". *[b] IPCC 4th report (Solomon, *et al*., 2007). *[c] Honeywell MSDS (2011). *[d] Koyama *et al*. (2012, 2013). *[e] Akasaka *et al*. (2013).

rather higher than the operating conditions of typical air conditioners. Table 2 compares the thermodynamic and transport properties between R1234ze(E) and R1234ze(Z) at saturation temperatures of 65 and 30 °C calculated with the REFPROP associated with the fluid file provided by Aakasaka *et al*. (2013).

The following two indices will be used to compare the predicted values. The bias, $\bar{\varepsilon}$, and standard deviation, σ, of predicted values from the experimental data are calculated as follows:

$$\bar{\varepsilon} = \frac{1}{n}\sum_{j=1}^{n}\varepsilon_j = \frac{1}{n}\sum_{j=1}^{n}\left[\left(\alpha_{\mathrm{cal},j} - \alpha_{\mathrm{exp},j}\right)/\alpha_{\mathrm{exp},j}\right] \text{ or } = \frac{1}{n}\sum_{j=1}^{n}\left[\left(\Delta P/\Delta Z_{\mathrm{cal},j} - \Delta P/\Delta Z_{\mathrm{exp},j}\right)/\left(\Delta P/\Delta Z_{\mathrm{exp},j}\right)\right] \quad (7)$$

$$\sigma = \sqrt{\frac{1}{n-1}\sum_{j=1}^{n}\left(\varepsilon_j - \bar{\varepsilon}\right)^2} \quad (8)$$

where n is the number of data points to be compared. The subscripts cal and exp indicate the prediction and the experiment.

3. RESULTS AND DISCUSSION

3.1 Condensation Test Results

Figure 3 plots the measured pressure gradient against the vapor quality for the condensing flow of R134a, R1234ze(E), and R1234ze(Z) at a saturation temperature of 65 °C and a heat flux of 10 kW m^{-2}. In Figure 3 (a) and (b), the symbols show the measured data at mass velocities of 150 kg $m^{-2}s^{-1}$ and 400 kg $m^{-2}s^{-1}$, respectively. The horizontal and vertical

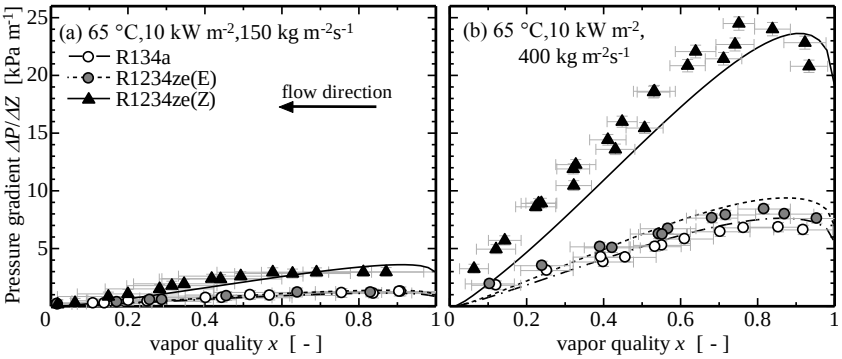

Figure 3: Condensation pressure gradient at 65 °C and 10 kWm^{-2}. Symbols are experimental pressure gradient; lines are predicted pressure gradient by Yonemoto and Koyama (2007).

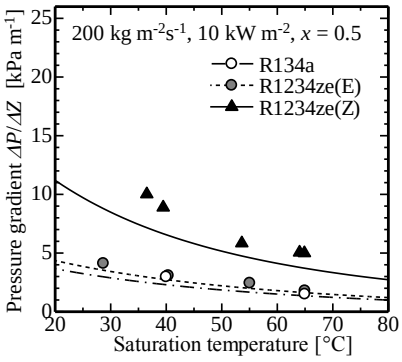

Figure 4: Variation in condensation pressure gradient against saturation temperature at a vapor quality of 0.5.

bars appended to the symbols show the propagated measurement uncertainty (Taylor, 1997) in the pressure gradient and the vapor quality change in the subsection. The lines are the pressure gradient predicted by the correlation of Yonemoto and Koyama (2007). As shown in Figures 3 (a) and (b), the maximum pressure gradient of R1234ze(Z) is approximately 2.7 times as high as that of R1234ze(E) and R134a at these conditions. This difference can be explained by the difference in the vapor density: the vapor densities of R1234ze(Z), R1234ze(E) and R134a are 28.6, 80.1 and 100 kg m^{-3}, respectively, at a saturation temperature of 65 °C. Due to these vapor densities, the volumetric flow rate of R1234ze(Z) is 2.8 times larger than that of R1234ze(E) and 3.5 times larger than that of R134a at the given mass velocity. Therefore, the momentum dissipated by the shear stress in R1234ze(Z) flow, which is principally detected as the pressure gradient, should be much larger than the dissipation for the other refrigerants.

Figure 4 shows the variation in pressure gradient of R134a, R1234ze(E), and R1234ze(Z) as a function of the saturation temperature at a mass velocity of 200 kg m^{-2}s^{-1} and vapor quality of approximately 0.5. The pressure gradient of each refrigerant monotonically decreases with increasing the saturation temperature. The vapor density increases towards the critical point, while the liquid viscosity decreases. These property changes predominantly reduce the pressure gradient, although this change is somewhat mitigated by the decreasing liquid density and increasing vapor viscosity.

Figure 5 shows the typical experimental data for the condensation heat transfer at a saturation temperature of 65 °C and a heat flux of 10 kW m^{-2}. Of the tested refrigerants, i.e., R134a, R1234ze(E), and R1234ze(Z), the experimentally quantified HTC are shown at mass velocities of 150 and 400 kg m^{-2}s^{-1} with symbols in Figures 5 (a) and (b), respectively. The symbols plot the experimental data with bars that vertically indicate the measurement uncertainties and horizontally indicate the quality change in a subsection. The lines are the HTC calculated using the correlations of Cavallini *et al*. (2009). The HTC of R1234ze(E) is approximately twice that of the others at higher vapor qualities, namely above 0.6, where the forced convection contribution should dominate heat transfer. This difference in HTC,

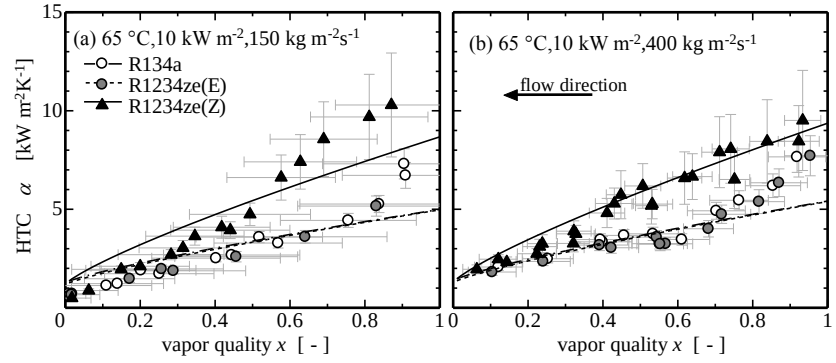

Figure 5: Condensation HTC at 65 °C and 10 kWm^{-2}. Symbols are experimental HTC: lines are predicted HTC by Cavallini *et al*. (2009).

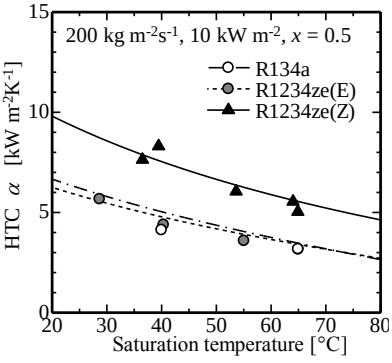

Figure 6: Variation in HTC against saturation temperature at a vapor quality of 0.5.

Table 3: Deviation of predicted pressure gradient and HTC from experimental data for condensation.

		R1234ze(Z)		R1234ze(E)		R134a	
		$\bar{\varepsilon}$	σ	$\bar{\varepsilon}$	σ	$\bar{\varepsilon}$	σ
$\Delta P/\Delta Z$	Cavallini *et al*. (1997)	0.08	0.22	0.13	0.25	0.12	0.17
	Goto *et al*. (2007, 2001)	-0.44	0.13	-0.37	0.13	-0.34	0.09
	Yonemoto and Koyama (2007)	-0.23	0.21	-0.20	0.24	-0.19	0.18
	Newell and Shah(2001)	0.31	0.45	-0.20	0.24	-0.27	0.18
HTC	Kedzierski and Goncalves (1999)	0.27	0.24	0.30	0.25	0.29	0.25
	Chamra *et al*. (2005)	-0.15	0.40	0.13	0.51	0.14	0.43
	Yonemoto and Koyama (2007)	0.05	0.25	0.01	0.20	-0.01	0.17
	Cavallini *et al*. (2009)	-0.08	0.27	0.05	0.26	0.05	0.24

which is more evident in the forced convection dominant region, can be rationalized with the difference in the vapor density, as is the case for the pressure gradient. The higher HTC of R1234ze(Z) is attributed mainly to the forced convective heat transfer due to a more than 2.8 times higher volumetric vapor flow rate of R1234ze(Z) comparing to the others. As listed in Table 1, the liquid thermal conductivity and the latent heat of vaporization of R1234ze(Z) is larger than that of the other refrigerants. The larger latent heat induces condensation heat transfer and the higher thermal conductivity decreases the thermal resistance in the liquid film. As a result of these and other effects, the condensation HTC of R1234ze(Z) exceeds those of R134a and R1234ze(E), especially at higher vapor qualities. The difference in the HTC between the tested refrigerants is well predicted by the correlation of Cavallini *et al*. (2009). Furthermore, several other correlations accurately predicted the HTC of these new refrigerants, as compared with the bias and the standard deviation in Table 3.

Figure 6 shows the variation in the condensation HTC as a function of the saturation temperature at 200 kg $m^{-2}s^{-1}$ and 10 kW m^{-2}. The experimental data represented by symbols were extracted from the data bank at a vapor quality ranging from 0.4 to 0.6. As the saturation temperature increases towards the critical point, the condensation HTC monotonically decreases. Kondou and Hrnjak (2012) confirmed this effect for CO_2 and R410A. According to their experimental verification, the condensation HTC of CO_2 and R410A in a horizontal smooth tube monotonically decreases as the saturation pressure increases up to a reduced pressure of 0.995. The trend demonstrated by the present experimental data is essentially identical to their remarks. Additionally, the correlation of Cavallini *et al*. (2009) shown with lines and some other correlations listed in Table 3 accurately predict this tendency for increasing saturation temperatures. As mentioned above, the selected correlations of condensation heat transfer were validated for the new refrigerants R1234ze(E) and R1234ze(Z) at saturation temperatures ranging from approximately 30 to 65 °C.

Figures 7 (a), (b), and (c) show the temperature distribution of the tube wall, namely the deviation in the measured tube wall temperature from the average value. The horizontal dashed lines are the threshold 0.2 K from the average. The vertical dashed line indicates the transition from an annular flow pattern to an intermittent flow pattern that was visually confirmed by El Hajal *et al*. (2003) and later modified by Olivier *et al*. (2007) for microfin tubes. The predicted transition point is very close to the point at which the tube wall temperature begins to deviate more than 0.2

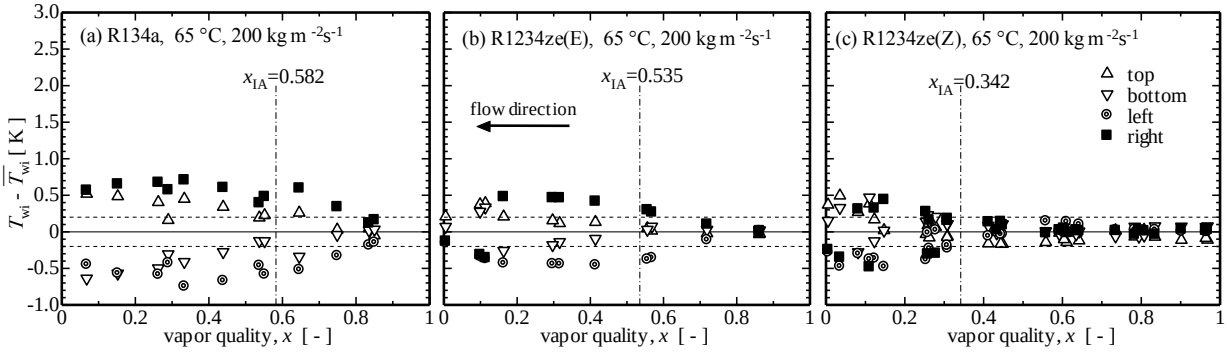

Figure 7: Temperature distribution of tube wall for condensation at 65 °C and 200 kg $m^{-2}s^{-1}$ (time-averaged).

K. If the temperature distribution indicates a flow pattern change indeed, Figure 7 demonstrates that R1234ze(Z) transitions to an intermittent flow at a lower vapor quality than the others. The correlation accurately predicts this change. The inertia force caused by the higher vapor appears to maintain the annular flow pattern in R1234ze(Z) condensing flow until a lower vapor quality is reached more readily than the other refrigerant flow. The prediction of El Hajal *et al*. (2003) with the modified coefficient of Olivier *et al*. (2007) seems to properly take into account the effect of refrigerant properties into the transition of the flow pattern.

3.2 Evaporation Test Results

Figure 8 plots the pressure gradient during the evaporation process at a saturation temperature of 30 °C and 10 kW m^{-2}. As with the condensation process, the pressure gradient of R1234ze(Z) is markedly higher than that of the others. At a mass velocity of 300 kg $m^{-2}s^{-1}$, the maximum pressure gradients of R134a and R1234ze(E) are 11 and 14 kPa m^{-1}, respectively. The maximum pressure gradient of R1234ze(Z) is 33 kPa m^{-1}, which is three times greater than that of R134a because of the higher vapor speed due to the smaller vapor density of R1234ze(Z).

Figure 9 shows the variation in the pressure gradient as a function of the saturation temperature. As with the case of condensation, the pressure gradients of all tested refrigerants, R134a, R1234ze(E), and R1234ze(Z), negatively correlate with the saturation temperature, while the pressure gradient of R134a and R1234ze(Z) consistently remains three times greater than that of R1234ze(Z) over the entire temperature range shown in Figure 9.

The aforementioned characteristics of the pressure gradient during the evaporation process are very similar to those during the condensation process. Hence, the same explanation for the vapor speed and liquid viscosity can be valid for evaporation, although the flow regime and the acceleration/deceleration due to phase changes should have dissimilar effects. Table 4 compares the predictions and experimental data for the pressure gradient and HTC of the evaporation process. The lines in Figures 8 and 9 and comparison in Table 4 indicate that the correlation by Kubota *et al*. (2001) accurately predicts the experimentally obtained pressure gradient.

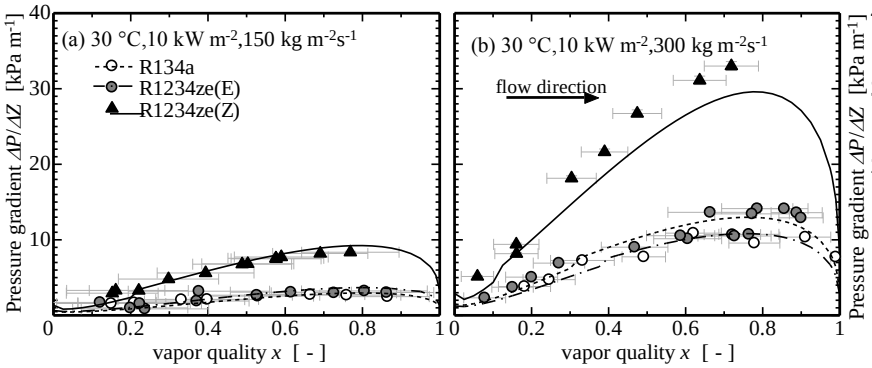

Figure 8: Evaporation pressure gradient at 30 °C and 10 kWm^{-2}. Symbols are experimental data: lines are predicted value by Kubota *et al*. (2001).

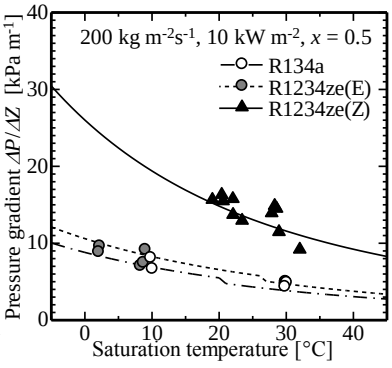

Figure 9: Variation in evaporation pressure gradient against saturation temperature at a vapor quality of 0.5.

Table 4: Deviation of predicted pressure gradient and HTC from experimental data for evaporation.

		R1234ze(Z)		R1234ze(E)		R134a	
		$\bar{\varepsilon}$	σ	$\bar{\varepsilon}$	σ	$\bar{\varepsilon}$	σ
$\Delta P/\Delta Z$	Goto *et al*. (2007, 2001)	-0.53	0.12	-0.37	0.12	-0.43	0.13
	Kubota *et al*. (2001)	-0.14	0.18	-0.06	0.18	-0.16	0.16
	Newell and Shah (2001)	0.73	0.68	-0.08	0.30	-0.26	0.28
	Filho *et al*. (2004)	-0.58	0.34	-0.75	0.20	0.13	0.79
HTC	Momoki *et al*. (1995)	-0.03	0.24	0.27	0.64	0.36	0.33
	Thome *et al*. (1997)	-0.20	-0.20	-0.26	0.46	-0.26	0.14
	Cavallini *et al*. (1998)	-0.06	0.21	0.03	0.62	0.04	0.15
	Mori *et al*. (2002)	-0.15	0.20	-0.02	0.48	-0.03	0.16

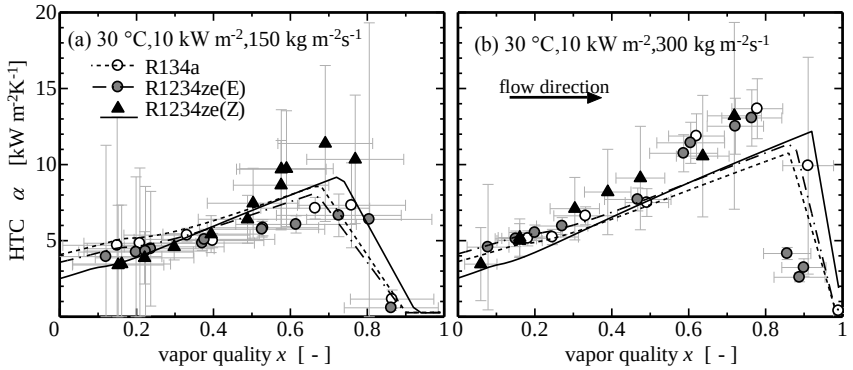

Figure 10: Condensation heat transfer at 65 °C and 10 kWm^{-2}. Symbols are experimental HTC: lines are predicted HTC by Cavallini *et al*. (1998) and Yoshida et al. (2000).

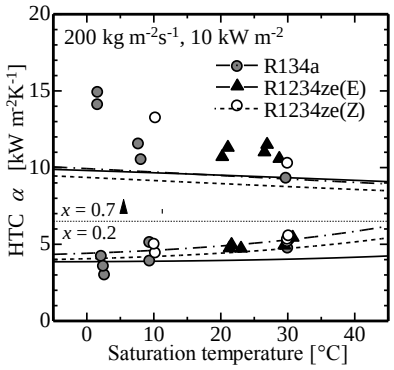

Figure 11: Variation in HTC against saturation temperature at a vapor quality of 0.5.

Figures 10 (a) and (b) plot the evaporation HTC at a saturation temperature of 30 °C, a heat flux of 10 kW m^{-2}, and mass velocities of 150 and 300 kg m^{-2}s^{-1}, respectively. The lines show the HTC predicted by the correlation of Cavallini *et al*. (1998) for the pre-dry out region, the HTC predicted by Yoshida *et al*. (2000) for the onset-dryout quality and the HTC predicted by Mori *et al*. (2000) for the post-dryout quality. At vapor qualities less than 0.2 where the nuclear boiling is most likely predominant, the HTC of R134a and R1234ze(E) are slightly higher than that of R1234ze(Z). At vapor qualities of approximately 0.7, just before the onset dryout where the forced convective evaporation should be dominant, the HTC of R134a and R1234ze(E) are lower than that of R1234ze(Z). These tendencies are more evident at a mass velocity of 150 kg m^{-2}s^{-1}. The reduced pressures of R134a, R1234ze(E) and R1234ze(Z) are 0.19, 0.16, and 0.06, respectively at a saturation temperature of 30 °C. Many previous studies remarked that refrigerants operating at lower reduced pressures yield lower nucleate boiling HTC values. These studies attributed the decrease in the nucleate boiling HTC to the larger bubble-departure-diameter required to balance the stronger surface tension. Conversely, the higher vapor speed of refrigerants at lower reduced pressures increases the forced convective evaporation HTC. The present HTC data illustrate this theory.

Figure 11 compares the variation in the HTC with saturation temperatures for R134a, R1234ze(E), and R1234ze(Z). The lines represent the HTC values predicted by the correlation of Cavallini *et al*. (1998). The symbols represent the experimental data for the HTC extracted from the databank at vapor qualities of approximately 0.2 and 0.7. Based on the above-mentioned theories, the HTC at a vapor quality of 0.2 positively correlates with the saturation temperature, while the HTC at a vapor quality of 0.7 negatively correlates with the saturation temperature. All tested refrigerants, R134a, R1234ze(E), and R1234ze(Z) showed the same tendency. Although the predicted HTC deviates from the experimental HTC at a vapor quality of 0.7 and saturation temperatures below 10, both the predicted and experimental data indicate the same pattern, which is identical to the theoretical pattern. Furthermore, the other correlations listed in Table 4 satisfactorily agree with the experimental HTC.

Figure 12 shows the circumferential temperature distributions of the tube wall. The vertical chained lines and x_A show

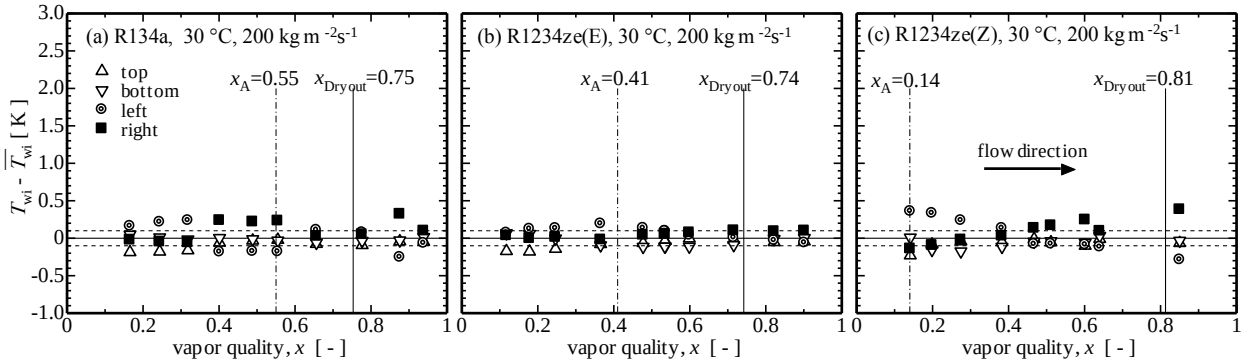

Figure 12: Temperature distribution of tube wall for evaporation at 30 °C and 200 kg m^{-2}s^{-1} (time-averaged).

the transition from stratified to annular flow, which is obtained from the correlation of Mori *et al*. (2002). The vertical solid lines and x_{Dryout} are the onset dryout quality calculated according to the correlation of Yoshida *et al*. (2000). The temperature distribution during the evaporation process is smaller than that during the condensation process. The liquid flow may be more turbulent in the presence of the nucleate bubbles, which obscures the liquid-vapor interface. Therefore, determining the transition of the flow pattern from the temperature distribution of the tube wall is difficult. Conversely, the onset-dryout quality is almost indistinguishable as the tube wall temperature distribution changes in Figures 12 (a) and (c). Beyond the onset-dryout quality, the temperature distribution seems to slightly grow. The right side shows the higher temperature; the left side shows lower temperature. This change is likely due to the liquid film flowing along the clockwise helical fins, where it begins to break from the right side.

4. CONCLUSIONS

The characteristics of the low GWP refrigerants R1234ze(E) and R1234ze(Z) in horizontal microfin tubes at higher temperatures were experimentally investigated in this study. For both the condensation and evaporation, the pressure gradient of R1234ze(Z) was approximately three times greater than those of R1234ze(E) and the conventional refrigerant R134a. For the condensation at 65 °C, the HTC of R1234ze(Z) was approximately 2.6 times higher than those of R1234ze(E) and R134a, especially at vapor qualities beyond 0.6. As the saturation temperatures increased, the condensation HTC monotonically decreased. For the evaporation at 30 °C, the HTC of R1234ze(Z) was slightly higher than those of R1234ze(E) and R134a at vapor qualities from 0.4 to the onset dryout quality, but slightly lower at vapor qualities less than 0.4. The evaporation HTC at a vapor quality less than 0.4, where nuclear boiling may dominate heat transfer, positively correlates with the saturation temperature. In contrast, the HTC at vapor qualities between 0.4 to the onset dryout, where convective evaporation may dominate, negatively correlates with the saturation temperature. The predicted pressure gradient and HTC agree well with the experimental data. The currently provided thermodynamic and transport properties and the existing correlations can accurately predict the pressure gradient and HTC of R1234ze(E) and R1234ze(Z).

NOMENCLATURE

D_o	outer diameter	(m)
P	pressure	(Pa)
Q	heat transfer rate	(W)
T	temperature	(°C)
Z	tube length	(m)
d_{eq}	equivalent inner diameter	(m)
h	enthalpy	(J kg^{-1})
n	number of data points	(-)
q	heat flux	(W m^{-2})
x	vapor quality	(-)
α	heat transfer coefficient	(W m^{-2}K^{-1})
ε	bias	(-)
η_A	surface enlargement	(-)
λ	thermal conductivity	(W m^{-1}K^{-1})
σ	standard deviation	(-)

Subscript

A	annular
Dryout	dryout
H2O	water
IA	intermittent-annular
TS	test section
cal	calculation
exp	experiment
i	inlet
o	outlet

tube	tube
wi	inner wall
wo	outer wall

REFERENCES

Akasaka, R., Higashi, Y., Koyama, S., 2013, A fundamental equation of state for low GWP refrigerant HFO-1234ze(Z), *Proc. 4th IIR Conference on Thermophysical Properties and Transfer Processes of Refrigerants*, Delft, The Netherlands, Paper No. TP-052.

Brown, J. S., Zilio, C., Cavallini, A., 2009, The fluorinated olefin R-1234ze(Z) as a high-temperature heat pumping refrigerant, *Int. J. Refrig.*, vol. 32: p. 1412-1422.

Brown, J. S., Zilio, C., Cavallini, A., 2010, Thermodynamic properties of eight fluorinated olefins refrigerant, *Int. J. Refrig.*, vol. 33: p. 235-241.

Cavallini, A., Del Col, D., Mancin, S., Rossetto, L., 2009, Condensation of Pure and Near-Azeotropic Refrigerants in Microfin Tubes: a new computational procedure, *Int. J. Refrig.*, vol. 32: p. 162-174.

Cavallini, A., Del Col, L. D., Longo, G. A., Rossetto, L., 1997, Pressure drop during condensation and vaporization of refrigerants inside enhanced tubes, *Heat and Technology*, vol. 15, no. 1: p. 3-10.

Cavalllini, A., DelCol, D., Longo, G.A., Rosset, L., 1998, Refrigerant vaporization inside enhanced tubes, *Proc. Heat Transfer in Condensation and Evaporation*, Eurotherm seminar, Grenoble, France: p. 222-231.

Chamra, L.M., Mago, P.J., Tan, M.O., Kung, C. C., 2005, Modeling of condensation heat transfer of pure refrigerants in micro-fin tubes, *Int. J. Heat Mass Transfer*, vol. 48: p. 1293-1302.

El Hajal, J., Thome, J.R., Cavallini, A., 2003. Condensation in horizontal tubes, part 1: two-phase flow pattern map, *Int. J. Heat Mass Transfer*, vol. 46: p. 3349-3363.

Filho, E.P.B., Jabardo, J. M. S., Barbieri, P.E.L., 2004, Convective boiling pressure drop of refrigerant R-134a in horizontal smooth and microfin tubes, *Int. J. Refrig.*, vol. 27, no. 8: p. 895-903.

Fukuda, S., Kondou, C., Takata, N., Koyama, S., 2014, Low GWP Refrigerants R1234ze(E) and R1234ze(Z) for high temperature heat pumps, *Int. J. Refrig.*, vol. 40: p. 161-173.

Goto, M., Inoue, N., Ishiwatari, N., 2001, Condensation and evaporation heat transfer of R410A inside internally grooved horizontal tubes, Int. J. Refrig., vol. 24, no. 7: p. 628-638.

Goto, M., Inoue, N., Ishiwatari, N., 2007, Answer to comments by M.M. Awad on "Condensation and evaporation heat transfer of R410A inside internally grooved horizontal tubes", Int. J. Refrig., vol. 30, no. 8: p. 1467.

Higashi, Y., Hayasaka, S., and Ogiya, S., 2013, Measurements of PvT properties vapor pressures, and critical parameters for low GWP refrigerant R-1234ze(Z), *Proc. 4th IIR Conference on Thermophysical Properties and Transfer Processes of Refrigerants*, Delft, The Netherlands, Paper No. TP-018.

Honeywell Material Safety Data Sheet, 2011, MSDS Number: HFO-1234ze JPN, ver. 10: p. 1-10.

Kedzierski, M. A., Goncalves, J. M., 1999, Horizontal Convective Condensation of Alternative Refrigerants within a Micro-Fin Tube, *Journal of Enhanced Heat Transfer*, vol. 6, no. 2-4: p. 161-178.

Kondou, C., Hrnjak, P.S., 2012, Condensation from Superheated Vapor Flow of R744 and R410A at Subcritical Pressures in a Horizontal Smooth tube, Int. J. Heat Mass Transfer, vol. 55: p. 2779-2791.

Koyama, S., Fukuda, S., Osafune, K., Akasaka, R., 2012, Development of low GWP refrigerants suitable for heat pump systems, *Proc. International Symposium of New Refrigerants and Environmental Technology 2012*, Kobe, Japan: p. 135-140.

Koyama, S., Higashi, T., Miyara, A., Akasaka, R., 2013. Research and development of low-GWP refrigerants suitable for heat pump systems. In: JSRAE Risk Assessment of Mildly Flammable Refrigerants-2012 Progress Report, JSRAE, Japan: p. 29-34.

Kubota, A., Uchida, M., Shikazono, N., 2001, Predicting Equations for Evaporation Pressure Drop Inside Horizontal Smooth and Grooved Tubes, *Trans. JSRAE*, vol. 18, no. 4: p. 29-37 (in Japanese).

Lemmon, E.W., Huber, M.L., McLinden, M.O., 2013, Reference Fluid Thermodynamic and Transport Properties - REFPROP Ver. 9.1, National Institute of Standards and Technology, Boulder, CO, USA.

Miyara, A., Fukuda, R., Kuriyama, T., 2013, Thermal conductivity of HFO and HFO+HFC mixtures at saturated liquid condition, *Proc. 4th IIR Conference on Thermophysical Properties and Transfer Processes of Refrigerants*, Delft, The Netherlands, Paper No. TP-033.

Momoki, S., Yu, J., Koyama, S., Fujii, T., Honda, H., 1995, A correlation for forced convective boiling heat transfer of refrigerants in a microfin tube, *Trans. JAR*, vol. 12, no. 2: p. 177-184 (in Japanese).

Mori, H., Yoshida, S., Kakimoto, Y., Ohishi, K., and Fukuda, K., 2000, Post-dryout heat transfer to a refrigerant flowing in horizontal evaporator tubes, *Trans. JSRAE*, vol. 4: p. 521-528 (in Japanese).

Mori, H., Yoshida, S., Koyama, S., Miyara, A., Momoki, S., 2002, Prediction of heat transfer coefficients for refrigerants flowing in horizontal spirally grooved evaporator tubes, *Proc. 14th JSRAE Annual Conf*., JSRAE: p. 97-100 (in Japanese).

Newell, T. A., Shah, R. K., 2001, An assessment of refrigerant heat transfer, pressure drop, and void fraction effects in micro fin tubes, *HVAC&R Research*, vol. 7, no. 2: p. 125-153.

Olivier, J., Liebenberg, L., Thome, J.R., Meyer, J., 2007, Heat transfer, pressure drop, and flow pattern recognition during condensation inside smooth, helical micro-fin, and herringbone tubes, *Int. J. Refrig*., vol. 30: p. 609-623.

Solomon, S., Qin, D., Manning, M., Chen, Z., Marquis, M., 2007, IPCC 2007 Annual Report 4th Climate Change 2007 - The Physical Science Basis, p. 210-216.

Taylor, J.T., 1997, *An introduction to error analysis*, 2nd ed., University science book.

Thome, J.R., Kattan, N., Favrat, D., 1997, Evaporation in microfin tubes: a generalized prediction model, *Proc. Convective Flow and Pool Boiling Conf*., Kloster Irsee, Germany, Paper no. VII-4.

Yonemoto R., Koyama S., 2007, Experimental study on condensation of pure refrigerants in horizontal micro-fin tubes: proposal of correlations for heat transfer coefficient and frictional pressure drop, *Trans. JSRAE*, vol. 24, no. 2: p. 139-148, (in Japanese).

Yoshida, S., Mori, H., Kakimoto, Y., and Ohishi, K., 2000, Dryout quality for refrigerants flowing in horizontal evaporator tubes, *Trans. JSRAE*, vol. 4: p. 511-520 (in Japanese).

ACKNOWLEDGMENTS

The work presented here was financially supported by the New Energy and Industrial Technology Development Organization (NEDO). The test tubes were kindly provided by Kobelco and Materials Copper Tube, Ltd.